unfavorable steric factor: the C–H and C–C bonds are much shorter than Si–H and Si–C bonds. The phenyl rings of Ph_3CH thus may interact repulsively with the PO_2H groups of the $P_2O_5H_2^{2-}$ ligands.

Interestingly, the reactivity of $^3Pt_2^*$ is comparable to that of $^3n\pi^*$ excited states of ketones possessing energies similar to $^3Pt_2^*$ (E_T = 57.7 kcal mol^{-1}).[8,11] For example, k_H for the reaction of the $^3n\pi^*$ state of benzophenone (E_T = 69 kcal mol^{-1})[32] with Bu_3SnH is 4.7 × 10^7 M^{-1} s^{-1}, whereas for biacetyl (E_T = 55 kcal mol^{-1})[32] the rate constant is 1.5 × 10^7 M^{-1} s^{-1}.[33] The radical-like behavior of the $d\sigma^*p\sigma$ triplet excited state of Pt_2 most likely is attributable to the unpaired electron in $d\sigma^*$, because this electron is strongly localized in the open axial coordination sites.[34] The role of the $d\sigma^*$ electron in the reactions of $^3Pt_2^*$ apparently is analogous to that of the singly occupied oxo-localized n electron in the $^3n\pi^*$ chemistry of organic carbonyl compounds.[32,33]

Experimental Section

Materials. $K_4[Pt_2(P_2O_5H_2)_4]\cdot 3H_2O$ was synthesized according to a standard procedure.[13] (Acetone was not used during the precipitation of the product, as it causes formation of a green impurity.) $[Bu_4N]_4[Pt_2(P_2O_5H_2)_4]$ was prepared from the potassium salt as described previously.[35] All hydrides were obtained from Aldrich except Ph_3GeH and Bu_3SnD (Strem). Fresh samples were used without further purification and were handled under nitrogen. Ph_3CH (Aldrich) was twice recrystallized from ethanol in the presence of charcoal. Tin hydrides were kept cold between experiments. Acetonitrile (Burdick & Jackson high purity solvent) and CD_3CN (Aldrich, Gold Label) were used as obtained; 2-methyltetrahydrofuran (Aldrich) was purified by the ketyl method, whereas propionitrile (Aldrich) was distilled from CaH_2.

Irradiations. Acetonitrile solutions containing $[Bu_4N]_4[Pt_2(P_2O_5H_2)_4]$ (typically (1.5–2.0) × 10^{-4} M) were degassed by freeze–pump–thawing. Stirred solutions were irradiated in a 10-mm cell, and the absorbance changes were measured in an attached 1-mm cell. A 1000-W Xe–Hg lamp was used as the irradiation source. Irradiations in the 370-nm region were performed by employing a combination of 0–52 cutoff and 7–39 band-pass Corning filters. (The transmittance profile of this filter combination is a nearly symmetrical band with a maximum at 370 nm and a 30-nm fwhm.) Oriel interference filters were used for monochromatic 436- and 313-nm irradiations. NMR samples were prepared by irradiation of the reactants in CD_3CN in 5-mm NMR tubes that were sealed under vacuum. A typical initial Pt_2 concentration for NMR measurements was in the range (5–8) × 10^{-3} M.

Instrumentation. Cary 17 and HP 8450A instruments were used to record the UV–vis absorption spectra. The emission spectra were obtained as described previously.[3] The excitation spectrum of $Pt_2(SnBu_3)_2$ was measured on a Perkin-Elmer MPF-66 spectrofluorimeter. Quenching experiments employed a Quanta Ray Nd-YAG (8-ns fwhm; 355-nm excitation) laser system.[36] NMR spectra were recorded on a Bruker WM 500-MHz instrument at the Southern California Regional NMR Facility. A Varian E-line Century Series X-band spectrometer was used for the EPR measurements. Dihydrogen was detected by a Du Pont 21 492B mass spectrometer. The gas phase above frozen (77 K) solutions was sampled.

Acknowledgment. We thank V. M. Miskowski, A. E. Stiegman, and D. C. Smith for helpful discussions. This research was supported by National Science Foundation Grants CHE84-19828 (H.B.G) and CHE84-40137 (Southern California Regional NMR Facility).

(32) Turro, N. J. *Modern Molecular Photochemistry*; Benjamin/Cummings: Menlo Park, NJ, 1978; p 290.
(33) Scaiano, J. C. *J. Photochem.* **1973/1974**, *2*, 81–118.
(34) (a) Vlček, Jr., A.; Gray, H. B. *J. Am. Chem. Soc.* **1987**, *109*, 286–287. (b) Similar H atom transfer reactivity has been observed for $Re(CO)_5$ and related mononuclear $d\sigma^*$-radical species: Hanckel, J. M.; Lee, K.-W.; Rushman, P.; Brown, T. L. *Inorg. Chem.* **1986**, *25*, 1852–1856.
(35) Stiegman, A. E.; Rice, S. F.; Gray, H. B.; Miskowski, V. M. *Inorg. Chem.* **1987**, *26*, 1112–1116.
(36) Nocera, D. G.; Winkler, J. R.; Yocom, K. M.; Bordignon, E.; Gray, H. B. *J. Am. Chem. Soc.* **1984**, *106*, 5145–5150.

Contribution from the Institut für anorganische Chemie, Universität Bern, CH-3000 Bern 9, Switzerland, and Department of Pure and Applied Chemistry, University of Strathclyde, Glasgow G1 1XL, U.K.

Spin Cluster Excitations in Ti^{2+}-Doped $MnCl_2$

Stuart M. Jacobsen,[†] Hans U. Güdel,*[†] and W. Ewen Smith[‡]

Received August 28, 1986

Single-crystal absorption spectra of Ti^{2+} as an impurity in $MnCl_2$ were recorded between 1.5 K and room temperature. A particular feature of these spectra is transitions to the low-energy ^1E_g level of Ti^{2+} in the near-infrared region that are spin-forbidden on the single center. These bands appear entirely as a result of magnetic exchange with the surrounding Mn^{2+} ions. A one-parameter model based on a $Ti^{2+}(Mn^{2+})_6$ spin cluster was used to characterize the spectra. An excellent agreement between theory and experiment was found with a value for the Ti^{2+}–Mn^{2+} exchange parameter of J = −6.2 cm^{-1}. The emission spectrum at 45 K was also found to agree with the predictions of the model. The lowest energy ground-state level is described by the function |15 14⟩, where 15 is the total spin of Mn^{2+} ions and 14 is the overall spin of the cluster.

1. Introduction

This paper examines the effect of replacing an ion in a magnetic host lattice with another magnetic ion that has a different spin quantum number. The system is a Ti^{2+} impurity in $MnCl_2$. A theoretical treatment based on a $Ti^{2+}(Mn^{2+})_6$ spin cluster is used to provide a quantitative explanation for the anomalous intensities and band shapes of formally forbidden Ti^{2+} spin-flip transitions found in the lowest energy near-infrared spectral region.

Ti^{2+} is the only divalent first-row transition-metal ion which, in fairly strong ligand-field environments, has the pure triplet → singlet absorption transition as the lowest energy one. As a consequence, it is possible to observe sharp line emission from the ^1E_g excited state to the $^3T_{1g}$ ground state when Ti^{2+} is incorporated into $MgCl_2$, by exciting the higher energy spin-allowed bands and allowing the excitation to decay nonradiatively to the ^1E_g state.[1] However, the complementary absorption bands of this Ti^{2+} spin flip (i.e. $^3T_{1g} \rightarrow {}^1E_g$) have never been observed in the spectrum of Ti^{2+} in $MgCl_2$. Even at low temperatures and high concentrations of Ti^{2+},[2,3] these absorption bands have remained elusive, and it has to be concluded that the transition moments are too low to allow observation in absorption. This situation is dramatically reversed, however, when the absorption spectrum of Ti^{2+} in $MnCl_2$ is examined.[4] Here, the low-energy spin-flip transitions are observed as sharp lines with larger ϵ values than those of the

*To whom correspondence should be addressed.
[†]Universität Bern.
[‡]University of Strathclyde.

(1) Jacobsen, S. M.; Smith, W. E.; Reber, C.; Güdel, H. U. *J. Chem. Phys.* **1986**, *84*, 5205.
(2) Wilson, D. R.; Brown, D. H.; Smith, W. E.; *Chem. Phys. Lett.* **1981**, *84*, 552.
(3) Wilson, D. R.; Smith, W. E. *Inorg. Chem.* **1986**, *25*, 898.
(4) Jacobsen, S. M.; Smith, W. E. *J. Phys. C* **1985**, *18*, L1031.

0020-1669/87/1326-2001$01.50/0

spin-allowed bands, even at room temperature. Therefore, it is obvious that Ti^{2+}–Mn^{2+} exchange interactions play an important role in the spectrum of Ti^{2+} in $MnCl_2$.

$MnCl_2$ is a layer lattice with the $CdCl_2$ structure. Adjacent metal layers are separated by two chloride layers, and the interactions between the layers are smaller than intralayer interactions. The metal ions occupy octahedral sites that are slightly trigonally distorted, the exact point symmetry being D_{3d}. The Ti^{2+} ions isomorphously replace the Mn^{2+} ions in the doped lattice. $MnCl_2$ undergoes two magnetic phase transitions to complex 3D ordered phases at 1.96 and 1.81 K.[5]

Mn^{2+} has $S = {}^5/_2$ so that the ground state is a spin sextet, and since all excited states are quartets and doublets, this makes all d–d transitions both spin- and parity-forbidden. Since the lowest energy transition of $MnCl_2$ is ${}^6A_{1g} \rightarrow {}^4T_{1g}$ occurring at an energy of approximately 18 700 cm^{-1}, this leaves a convenient "window" below this energy to study the spectrum of the Ti^{2+} dopant ion.

2. Experimental Section

$MnCl_2$ was prepared by melting together stoichiometric amounts of anhydrous $ZnCl_2$ (BDH AnalaR) and manganese metal powder (Johnson Matthey Specpure) in a closed quartz tube that had been evacuated. The tube was heated at 800 °C for 24 h in an electrical furnace until all of the zinc was reduced to zinc metal, which settled at the bottom as an immiscible layer. On cooling, polycrystalline manganese chloride was recovered, which was separate from the slug of solid zinc metal formed.

The crystal of Ti^{2+} in $MnCl_2$ was grown from the melt by the Bridgman technique using the above in situ method. Ti^{2+} ions were doped into the host by melting $MnCl_2$ with the desired amounts of $ZnCl_2$ and titanium metal powder (Johnson Matthey Specpure) to produce Ti^{2+} ions and zinc metal. The titanium concentration was determined colorimetrically.

$MnCl_2$ cleaves readily along the planes perpendicular to the principal c axis. Samples for spectroscopy were cleaved along this plane with a razor blade to form sections about 0.5 mm thick by about 1 cm in diameter. In all spectroscopic measurements, therefore, the incident light was parallel to the principal axis.

Overall spectra were obtained on a Beckman Acta IV spectrometer by mounting the sample on an Air Products Displex unit for temperatures down to 10 K. High-resolution absorption experiments in the near-infrared region were performed as follows. Light from a 150-W quartz-halogen lamp was dispersed by a ${}^3/_4$-m Spex 1702 monochromator. After passing through a tuning-fork chopper, the near-infrared radiation was detected by a cooled (77 K) PbS cell. The signal was recorded by using a PAR 186A lock-in amplifier. An Oxford Instruments cryostat was used for low temperatures (down to 1.5 K).

The luminescence was excited by a 150-W xenon lamp, dispersed by the Spex 1702, and detected with the cooled PbS cell.

In all high-resolution experiments, data acquisition and monochromator control were performed by a Tektronix 4052A microcomputer system.

3. Theoretical Model

The central Ti^{2+} ion has six Mn^{2+} nearest neighbors, which are connected by bridging chlorides via an edge-sharing octahedral arrangement (Figure 1). That such an arrangement of paramagnetic ions can be regarded as a giant spin cluster has previously been suggested for the system Ni^{2+} in MnI_2.[6] This concept is based on the assumption that the Ti^{2+}–Mn^{2+} exchange is much larger than the Mn^{2+}–Mn^{2+} exchange. This is the case, which we would expect on theoretical grounds,[7] as well as from a comparison with Ni^{2+}–Mn^{2+} and Mn^{2+}–Mn^{2+} pairs in $KZnF_3$.[8] Although a direct measurement of J_{Mn-Mn} for $MnCl_2$ has not been reported in the literature, a value of −0.06 cm^{-1} has been estimated from the asymptotic Curie temperature.[9] From the optical spectra of Mn^{2+} pairs in $CdCl_2$, a value for the $Mn_2Cl_{10}^{6-}$ dimer of −0.7 cm^{-1} is calculated,[10] and it is safe to assume that J_{Ti-Mn} is at least

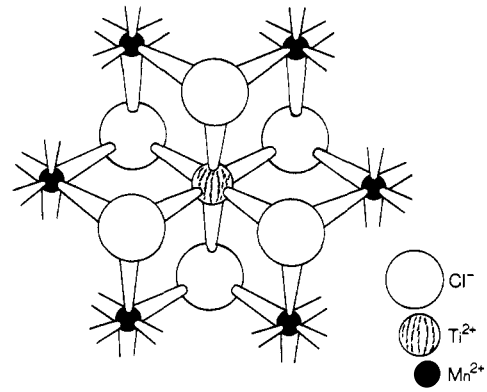

Figure 1. View of the $Ti^{2+}(Mn^{2+})_6$ cluster when Ti^{2+} is introduced as an impurity in $MnCl_2$. This view illustrates the layer of cations that are perpendicular to the c axis. The magnetic exchange interactions are expected to be strong between the central titanium and the six surrounding manganese ions but weaker between adjacent manganese ions. This allows the latter interactions to be neglected as well as the Mn^{2+}–Mn^{2+} interactions with the rest of the lattice.

an order of magnitude larger than J_{Mn-Mn}. A posteriori proof of the correctness of the assumption is provided by the value of J_{Ti-Mn} determined in this paper (section 5).

The ground state of Ti^{2+} in this crystal environment is orbitally nondegenerate ${}^3A_{2g}$ (D_{3d} notation), with the other trigonal component ${}^3E_g$ lying several hundred wavenumbers higher in energy.[1] A Heisenberg operator is therefore adequate to describe the ground-state splitting of the $Ti^{2+}(Mn^{2+})_6$ cluster, since Mn^{2+} is also a spin-only ion. Neglecting Mn^{2+}–Mn^{2+} interactions, there is only one parameter, J_{Ti-Mn}, which is abbreviated as J in the following:

$$\hat{H}_{cluster} = -2J(\vec{S}_0\cdot\vec{S}_1 + \vec{S}_0\cdot\vec{S}_2 + \vec{S}_0\cdot\vec{S}_3 + \vec{S}_0\cdot\vec{S}_4 + \vec{S}_0\cdot\vec{S}_5 + \vec{S}_0\cdot\vec{S}_6) \quad (1)$$

where $\vec{S}_0$ denotes the Ti^{2+} spin ($S_0 = 1$) and $\vec{S}_i$ ($i = 1$–6) denotes the spins of the nearest-neighbor Mn^{2+} ions ($S_i = {}^5/_2$).

The eigenvalues of the Hamiltonian (1) are easily obtained in closed form by the coupling scheme

$$\vec{S}_a = \vec{S}_1 + \vec{S}_2 + \vec{S}_3 + \vec{S}_4 + \vec{S}_5 + \vec{S}_6 \qquad \vec{S} = \vec{S}_a + \vec{S}_0 \quad (2)$$

in which $\vec{S}_a$ is the total spin of the $(Mn^{2+})_6$ cluster and $\vec{S}$ the total spin of the $Ti^{2+}(Mn^{2+})_6$ cluster. As a result of the high hexagonal symmetry, the energies of the cluster levels only depend on the two quantum numbers S_a and S. We designate these levels as $|S_a\ S\rangle$, and their energies are given by

$$E(S_a\ S) = -J[S(S+1) - S_a(S_a+1) - S_0(S_0+1)] \quad (3)$$

S_a values range from 0 to 15 and S values from $|S_a - 1|$ to $S_a + 1$. We thus obtain 32 cluster levels, which are listed with their energies and degeneracies in Table I.

Several features characteristic of such a large cluster with high symmetry are worth pointing out here.

The energy spacing is regular with an interval of $2J$ between adjacent levels. This is in contrast to a Ti^{2+}–Mn^{2+} pair, for example, which obeys a more conventional Landē splitting pattern. The lowest energy level in our cluster is found to be $|S_a\ S\rangle = |15\ 14\rangle$. Intuitively this makes sense, because this level contains the function $|S_a\ M_{sa}\ S_0\ M_{so}\rangle = |15\ 15\ 1\ -1\rangle$, which corresponds to parallel spins of all six Mn^{2+} ions and an antiparallel spin on the Ti^{2+} ion, thus giving overall antiferromagnetism. The least stable level, on the other hand, is $|S_a\ S\rangle = |15\ 16\rangle$, containing the function $|S_a\ M_{sa}\ S_0\ M_{so}\rangle = |1\ 15\ 1\ 1\rangle$ and thus corresponding to ferromagnetic alignment of all of the spins. As a result of the neglect of Mn^{2+}–Mn^{2+} interactions, all levels with $S_a = S$ have the same energy.

The degeneracies of the cluster levels are perhaps even more interesting, because they are indicative of how such a cluster model

(5) Regis, M.; Farge, Y. *J. Physique (Les Ulis, Fr.)* **1976**, *37*, 627.
(6) Hoekstra, H. J. W. M.; Ronda, C. R.; Haas, C. *Physica B* **1983**, *122*, 295.
(7) Gondaira, K. I.; Tanabe, Y. *J. Phys. Soc. Jpn.* **1966**, *21*, 1527.
(8) Ferguson, J.; Guggenheim, H. J.; Tanabe, Y. *J. Chem. Phys.* **1966**, *45*, 1134.
(9) (a) Starr, C.; Bitter, F.; Kaufman, A. R. *Phys. Rev.* **1940**, *58*, 977. (b) Hoekstra, H. J. W. M.; Haas, C. *Physica B+C (Amsterdam)* **1985**, *128B+C*, 327.
(10) McCarthy, P. J.; Güdel, H. U. *Inorg. Chem.* **1986**, *25*, 838.

Table I[a]

S_a	$N(S_a)$	$E(S_a S)$	$\|S_a S\rangle$	degeneracy $(2S+1)\cdot N(S_a)$	levels where $S_a = S$	degeneracy $(2S+1)\cdot N(S_a)$
15	1	-30J	| 15 16⟩	33	| 15 15⟩	31
14	5	-28J	| 14 15⟩	155	| 14 14⟩	145
13	15	-26J	| 13 14⟩	435	| 13 13⟩	405
12	35	-24J	| 12 13⟩	945	| 12 12⟩	875
11	70	-22J	| 11 12⟩	1 750	| 11 11⟩	1 610
10	126	-20J	| 10 11⟩	2 898	| 10 10⟩	2 646
9	204	-18J	| 9 10⟩	4 284	| 9 9⟩	3 876
8	300	-16J	| 8 9⟩	5 700	| 8 8⟩	5 100
7	405	-14J	| 7 8⟩	6 885	| 7 7⟩	6 075
6	505	-12J	| 6 7⟩	7 575	| 6 6⟩	6 565
5	581	-10J	| 5 6⟩	7 553	| 5 5⟩	6 391
4	609	- 8J	| 4 5⟩	6 699	| 4 4⟩	5 481
3	575	- 6J	| 3 4⟩	5 175	| 3 3⟩	4 025
2	475	- 4J	| 2 3⟩	3 325	| 2 2⟩	2 375
1	315	- 2J	| 1 2⟩	1 575	| 1 1⟩	945
0	111	0J	| 0 1⟩	333	| 0 0⟩	111
		+ 2J	$\|S_a = S\rangle$	46 656		46 656
		+ 4J	| 1 0⟩	315		
		+ 6J	| 2 1⟩	1 425		
		+ 8J	| 3 2⟩	2 875		
		+10J	| 4 3⟩	4 263		
		+12J	| 5 4⟩	5 229		
		+14J	| 6 5⟩	5 555		
		+16J	| 7 6⟩	5 265		
		+18J	| 8 7⟩	4 500		
		+20J	| 9 8⟩	3 468		
		+22J	|10 9⟩	2 394		
		+24J	|11 10⟩	1 470		
		+26J	|12 11⟩	805		
		+28J	|13 12⟩	375		
		+30J	|14 13⟩	135		
		+32J	|15 14⟩	29		

[a] In the left-hand column S_a is the possible spins of the $(Mn^{2+})_6$ cluster and $N(S_a)$ is the number of ways of arranging these spins. The center column gives the energies ($E(S_a S)$) and degeneracies of all 32 functions in the $Ti^{2+}(Mn^{2+})_6$ spin cluster. The right-hand column shows how the individual degeneracies of functions for which $S_a = S$ are obtained. These are then totaled and used in the highly degenerate function $S_a = S$ (center column).

might merge into a spin-wave model if the cluster size is increased. The normal spin multiplicity ($2S + 1$) has to be multiplied by $N(S_a)$, the number of different possible ways of coupling individual Mn^{2+} to produce S_a, in order to obtain the true degeneracy of a cluster level $|S_a S\rangle$. As can be seen in Table I, the resulting degeneracies span a range from 29 to 46 656. A plot of this "density of states" vs. energy is included in Figure 4. The picture consists of a singularity at $E(S_a = S) = 2J$, accompanied by a high-energy and a low-energy wing, each of them spanning approximately 200 cm^{-1}. The two wings are not symmetrical, the low energy one having a greater weighting.

From luminescence studies of Ti^{2+} in the related trigonal lattice $MgCl_2$, we infer that the lowest excited state is ^1E_g in D_{3d}.[1] This state derives from the same electron configuration $(t_{2g})^2$ as the ground state, at least in an octahedral approximation. The intraconfigurational nature of the transition explains its sharpness. The spin moment of Ti^{2+} is zero in the excited state. As a consequence $S_a = S$ for all cluster levels of this state, and since we are neglecting J_{Mn-Mn}, all levels have the same energy with a total spin degeneracy of 46 656, the same as for the $S_a = S$ ground-state levels.

The relevant selection rules for cluster transitions arising through an exchange mechanism are

$$\Delta S = 0 \qquad \Delta M_s = 0 \tag{4}$$

The transition of interest is spin-forbidden in the single Ti^{2+} ion. In the cluster, the excitation can be considered as a spin flip within the $(t_{2g})^2$ configuration of Ti^{2+} accompanied by a proper spin deviation on the surrounding $(Mn^{2+})_6$ cluster. The resulting selection rules with regard to the surrounding cluster are thus

$$\Delta S_a = \pm 1, 0 \qquad \Delta M_{sa} = \pm 1, 0 \tag{5}$$

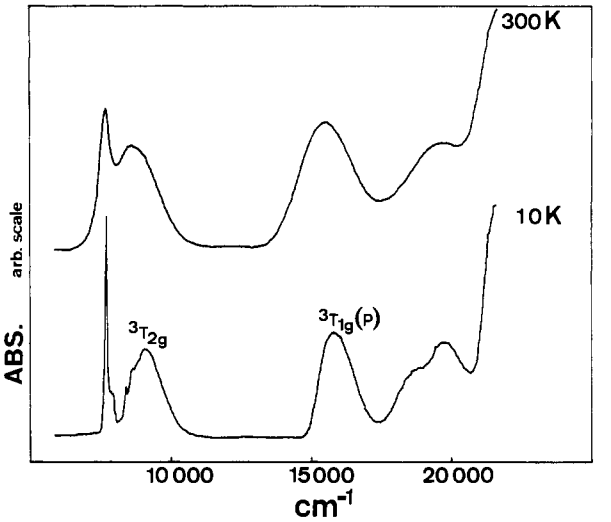

Figure 2. Overall spectra at 300 and 10 K of a crystal of $MnCl_2$ with a 1% replacement of Ti^{2+} ions. The base lines of these spectra are staggered for clarity. All bands below 17 500 cm^{-1} are due to the Ti^{2+} dopant. The sharp band in the low-energy region is an exchange-induced transition to the ^1E_g excited state of Ti^{2+} (see text for details).

During the excitation from the ground state to the excited state, the Ti^{2+} ion decouples from the surrounding $(Mn^{2+})_6$ cluster. Conversely, in the emission process the magnetic moment of Ti^{2+} must be very rapidly "switched on". We are presently investigating the important question of whether the spins of the surrounding $(Mn^{2+})_6$ have enough time to couple to the Ti^{2+} spin in this process.

4. Spectroscopic Results

The overall spectrum of a crystal of $MnCl_2$ containing a 1% replacement of Mn^{2+} by Ti^{2+} is given in Figure 2. All absorption bands below 17 500 cm^{-1} are due to the Ti^{2+} dopant ion. The two spin-allowed transitions expected for an octahedral d^2 ion, i.e. $^3T_{1g} \rightarrow {}^3T_{2g}$ and $^3T_{1g} \rightarrow {}^3T_{1g}$ (P), are observed at 9090 and 15 820 cm^{-1}, respectively (10 K). From this, values for the ligand-field parameters Dq = 1000 cm^{-1} and B = 520 cm^{-1} are calculated (C/B = 4.42). In this paper we shall focus our attention on the low-energy region of the spectrum where the spin-flip transitions of Ti^{2+} within the $(t_{2g})^2$ configuration are observed. Figure 2 shows that these spin flips occur in the energy region 7500–8800 cm^{-1} and are narrower at 10 K than at room temperature, but even at room temperature the ϵ value is greater than those of the two spin-allowed transitions, although this is not true of the oscillator strengths.

Examination of the high-resolution spectra in the near-infrared region between 1.5 and 120 K (Figure 3) shows that the most intense absorption exhibits considerable temperature dependence. At 1.5 K this band is at 7773 cm^{-1}, but on going to higher temperatures, it loses intensity, broadens, and shifts its maximum intensity position to lower energies. Between 1.5 and 120 K this energy shift is 89 cm^{-1}. A second feature of the spectrum at higher temperatures is the appearance of a hot band at 7586 cm^{-1}. The hot band's behavior is quite different from that of the main band. Between 60 and 120 K it gains intensity, but its breadth and energy position do not change within experimental error. Below 10 K there are additional, weak bands ranging in energy from 7651 to 8119 cm^{-1}, with the most intense at 7998 cm^{-1}.

Since the near-infrared transitions are the lowest energy ones, it is also possible to do luminescence experiments. For this particular system luminescence is a very useful technique since it gives a direct picture of the ground state and is not dependent on the thermal population of ground-state sublevels. The luminescence spectrum at 45 K (Figure 4) shows a strong, sharp emission band that coincides with the hot band in absorption. There are broader features on both the high- and the low-energy sides of this prominent band. The high-energy wing is rather weak and covers the same energy range as the broad absorption band at 60 K (Figure 4).

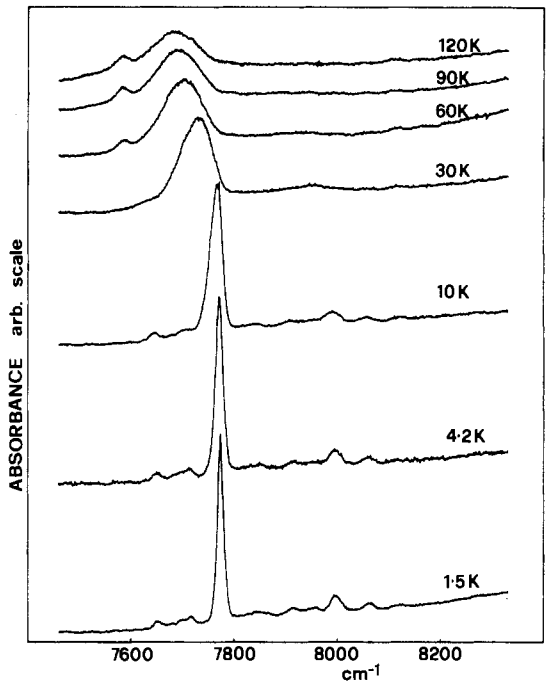

Figure 3. High-resolution near-infrared spectra of Ti^{2+} in $MnCl_2$ showing temperature dependence between 1.5 and 120 K. Base lines of all spectra are staggered.

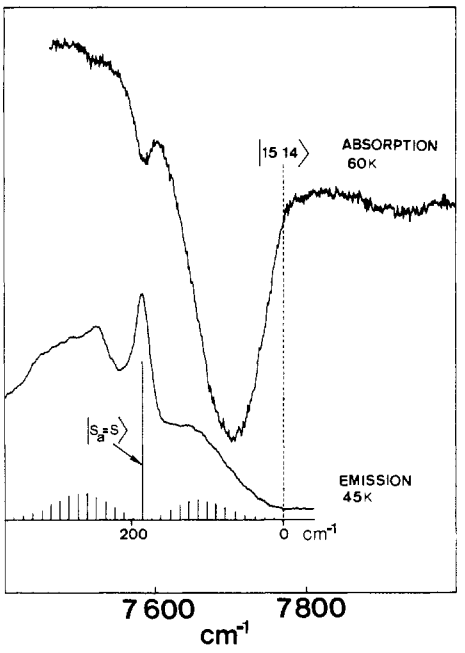

Figure 4. Absorption spectrum (60 K) and emission spectrum (45 K) of Ti^{2+} in $MnCl_2$ in the near-infrared region. Note that the absorption spectrum in this figure is intensity-reversed compared to absorption spectra in other figures, as this allows a more meaningful comparison with the emission spectrum. The broken vertical line indicates the energy position of the |15 14⟩ ground-state level in both absorption and emission. The inset below the emission spectrum is a graphical representation of the density of states for the ground-state manifold of the $Ti^{2+}(Mn^{2+})_6$ cluster. Note that these states have absolute energy units here and are shifted by $32J$ compared with values in Table I.

5. Discussion

In this section we discuss the spectroscopic results in terms of the model presented in section 3. At 1.5 K the lowest energy ground-state level |15 14⟩ is expected to have a high population despite its low degeneracy. The main absorption band at this temperature has an energy of 7773 cm^{-1} and a width of 15 cm^{-1}. We assign it to the transition |15 14⟩ ($^3A_{2g}$) → |$S_a = S$⟩ (^1E_g).

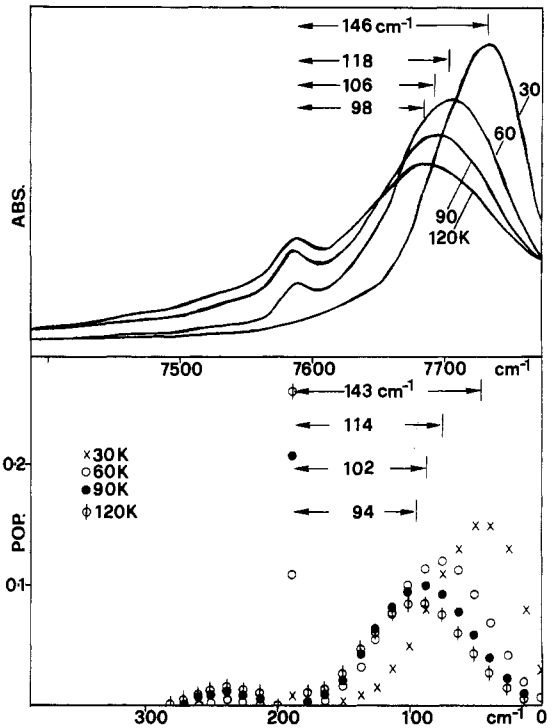

Figure 5. Bottom: Theoretical populations of the ground-state manifold of $Ti^{2+}(Mn^{2+})_6$ at various temperatures, along with the expected energy separations between the density of states absorption band and the $S_a = S$ band. Note that these states have the x axis in absolute energy units and are shifted by $32J$ compared with values in Table I. Top: Experimental absorption spectra for these temperatures along with the actual energy separations found.

The shift to lower energy and broadening of the absorption band with increasing temperature are the result of populating higher energy levels of the ground state. Due to the strongly increasing degeneracies, the higher levels become appreciably populated even at 30 K. The energy difference between adjacent cluster levels is obviously smaller than the bandwidths of the individual transitions, so that the latter are not resolved in the spectrum. By neglecting Mn^{2+}–Mn^{2+} exchange in our model, one sees that all levels |$S_a = S$ = 0–15⟩ in the ^1E_g excited state are degenerate. This is a rather crude approximation, and the observed bandwidth of 15 cm^{-1} at 1.5 K may have a dominant contribution from the excited-state splitting. However, this does not affect the basic assumptions of our further discussion.

At 60 K and higher temperatures we observe the relatively sharp hot band at 7586 cm^{-1}. It is displaced from the 1.5 K origin by 187 cm^{-1}. This rather large displacement and the fact that the band is clearly seen at 60 K imply that the band originates in a ground-state level with a singularly high degeneracy. From Table I we see that our cluster model offers exactly what we need: the highly degenerate levels |$S_a = S$ = 0–15⟩. The assignment of the 7586-cm^{-1} band to the transitions |$S_a = S$ = 0–15⟩ ($^3A_{2g}$) → |$S_a = S$ = 0–15⟩ (^1E_g) is thus straight forward, and we can equate the observed energy difference of 187 cm^{-1} to $-30J$, leading to a J value of -6.2 cm^{-1}.

With this value of J and the degeneracies of Table I, we can now calculate thermal populations of all ground-state levels for different temperatures. This is illustrated in the lower half of Figure 5 for temperatures of 30, 60, 90, and 120 K. An excellent correlation is found between these populations and the absorption band shapes and positions at the same temperature (upper half of Figure 5). The observed energy separations between the sharp hot band and the maximum of the broad band differ from the calculated values by less than 5 cm^{-1} at all temperatures. This agreement is remarkable. It shows that the density of states completely determines the intensity distribution. Transition matrix elements are not determinant. Transition probabilities must

average to the same value for the various sets of degenerate levels.

The emission spectrum at 45 K fits very nicely into this picture. The main sharp band, which coincides with the hot absorption band at 7586 cm^{-1}, is assigned to the transitions $|S_a = S = 0–15\rangle$ (^1E_g) → $|S_a = S = 0–15\rangle$ ($^3A_{2g}$). In addition, the two broad wings on the low- and high-energy sides of this peak contain the overlapping transition to the other levels of the ground-state multiplet. The density of states for the ground-state manifold is plotted underneath the emission spectrum in Figure 4. The correlation with the experimental intensity distribution is excellent on the high-energy side of the $|S_a = S\rangle$ central peak. On the low-energy side the correlation is less perfect. In this spectral region there is a superposition of additional bands, which grow in intensity with decreasing temperature. These bands cannot be explained within the framework of the present model. They are most likely transitions to spin configurations different from the relaxed ground-state discussed in this paper, and these spin configurations may well originate from higher order lattice effects as T_N of $MnCl_2$ is reached. We are presently engaged in a more detailed study of these effects.

The effects observed here as well as the formalism used for their interpretation have a certain analogy to the magnon sidebands observed in the optical spectra of magnetically ordered compounds.[11] Positions and shapes of magnon sidebands are determined by the energy dispersion, i.e. the strength of the exchange coupling and the density of magnon states.

Finally we turn to a brief discussion of the weak sidebands observed below 10 K in the high-resolution absorption spectra (Figure 3). The most intense band at 7998 cm^{-1} (1.5 K), which is separated by 225 cm^{-1} from the main band, could be an a_{1g} vibrational sideband of the electronic origins. This is supported by the observed shift to lower energy between 10 and 30 K, which parallels the shift of the main band. The weak bands on the low-energy side of the main peak in the 1.5 K spectrum, which cannot be vibrational sidebands, are attributed to slightly perturbed Ti^{2+} centers. Nearest- and next-nearest-neighbor Ti^{2+} pairs, which are present in small concentrations in a crystal with 1% Ti^{2+}, are the most likely candidates.

(11) Sell, F. D.; Greene, R. L.; White, R. M. *Phys. Rev.* **1967**, *158*, 489.

6. Conclusions

The main near-infrared spectroscopic features of Ti^{2+} in $MnCl_2$ are explained remarkably well by using the one-parameter spin cluster model with $J = -6.2$ cm^{-1}. The fact the Ti^{2+}–Mn^{2+} interactions are 1–2 orders of magnitude larger than the Mn^{2+}–Mn^{2+} interactions is probably one of the main reasons for the success of the model. The model could thus potentially be applied to other systems of paramagnetic ions in paramagnetic host lattices, provided that the dopant–host interactions are the dominant ones. To the chemist, such a molecular approach to a solid-state problem is conceptually a very attractive one. The system of Ti^{2+} as an impurity in $MnCl_2$ offers advantages over other such magnetic host systems that have caught the attention of workers in this field, e.g. Ni^{2+} in MnI_2[6] and Cr^{3+} in $GdAlO_3$.[12–14] Since the formally spin-forbidden absorptions of Ti^{2+} have little or no single-ion intensity and are completely exchange-induced, there is no ambiguity as to which mechanism is the dominant one. Also the fact that Ti^{2+} has zero spin in the excited state greatly simplifies both the theoretical treatment and the experimental assignment of absorption bands. In addition, the system is well suited to luminescence studies, which provide an extra method of probing the ground-state properties.

Acknowledgment. We are grateful to the Royal Society for a fellowship under the European Science Exchange Programme (to S.M.J.).

(12) Helman, J. S.; Baltensperger, W. *Phys. Rev. B: Condens. Matter* **1982**, *25*, 6847.
(13) Aoyagi, K.; Kajiura, M.; Sugano, S. *J. Phys. Soc. Jpn.* **1981**, *50*, 3725.
(14) Kita, T.; Tanabe, Y. *J. Phys. Soc. Jpn.* **1985**, *54*, 2293.

Contribution from the Department of Chemistry, Univeristy of Michigan, Ann Arbor, Michigan 48109

Relativistically Parametrized Extended Hückel Calculations. 11. Energy Bands for Elemental Tellurium and Polonium

Lawrence L. Lohr

Received October 9, 1986

An extension of the REX relativistically parametrized extended Hückel LCAO molecular orbital method to periodic solids is outlined. The method provides a simple and systematic approach to the description of the spin–orbit splitting of energy bands. The method is illustrated with results for the main-group elements tellurium and polonium, with trigonal-helical and simple-cubic structures, respectively. The helical structure of tellurium is described as a distortion of a simple-cubic structure, with the distortion being quenched in the case of polonium by its very large spin–orbit coupling.

Introduction

In 1979 we outlined[1] a relativistically parametrized version entitled REX of the extended Hückel molecular orbital method. The method differs from standard extended Hückel schemes[2,3] in that it employs an atomic $|lsjm\rangle$ complex spin–orbital basis rather than a real basis without spin. This complex basis, when combined with the standard Hückel assumption of effective Hamiltonian matrix elements being proportional to the corresponding overlap matrix elements, permits the systematic incorporation of spin–orbit coupling into the calculations. In addition the energy parametrization and choice of orbital exponents may be taken to reflect the other two important relativistic effects[4,5] in atomic structure, namely the contraction and stabilization of those orbitals of low total angular momentum, particularly $s_{1/2}$ and $p_{1/2}$ levels, and the self-consistent expansion and destabilization of those orbitals of high total angular momentum. The REX method[1,6] has been used in a number of studies[7–15] of the electronic

(1) Lohr, L. L.; Pyykkö, P. *Chem. Phys. Lett.* **1979**, *62*, 333.
(2) Hoffmann, R. *J. Chem. Phys.* **1963**, *39*, 1397.
(3) Howell, J.; Rossi, A.; Wallace, D.; Haraki, K.; Hoffmann, R. *QCPE* **1973**, *10* (Suppl.), 344.
(4) Pitzer, K. S. *Acc. Chem. Res.* **1979**, *12*, 271.
(5) Pyykkö, P.; Desclaux, J. P. *Acc. Chem. Res.* **1979**, *12*, 276.
(6) Lohr, L. L.; Hotokka, M.; Pyykkö, P. *QCPE* **1980**, *12*, 387.
(7) Lohr, L. L.; Hotokka, M.; Pyykkö, P. *Int. J. Quantum Chem.* **1980**, *18*, 34.
(8) Pyykkö, P.; Lohr, L. L. *Inorg. Chem.* **1981**, *20*, 1950.
(9) Pyykkö, P.; Wiesenfeld, L. *Mol. Phys.* **1981**, *43*, 557.

0020-1669/87/1326-2005$01.50/0